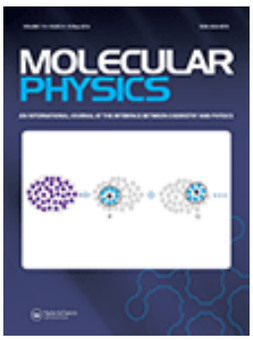

Taylor & Francis
Taylor & Francis Group

Molecular Physics

An International Journal at the Interface Between Chemistry and Physics

ISSN: 0026-8976 (Print) 1362-3028 (Online) Journal homepage: http://www.tandfonline.com/loi/tmph20

Ionisation energy, electron affinity, and mass spectral decomposition mechanisms of RDX isomers upon electron attachment and electron ionisation

F. A. Akin

To cite this article: F. A. Akin (2016): Ionisation energy, electron affinity, and mass spectral decomposition mechanisms of RDX isomers upon electron attachment and electron ionisation, Molecular Physics, DOI: 10.1080/00268976.2016.1246759

To link to this article: http://dx.doi.org/10.1080/00268976.2016.1246759

MOLECULAR PHYSICS, 2016
http://dx.doi.org/10.1080/00268976.2016.1246759

Taylor & Francis
Taylor & Francis Group

RESEARCH ARTICLE

Ionisation energy, electron affinity, and mass spectral decomposition mechanisms of RDX isomers upon electron attachment and electron ionisation

F. A. Akin

Department of Chemistry, Boğaziçi University, Bebek, Istanbul/Turkey

ABSTRACT

The structures, ionisation energies (IE), and electron affinities (EA) of 1,3,5-trinitro-1,3,5-triazacyclohexane (RDX) isomers upon loss and gain of an electron were calculated using density functional theory (DFT) methods. The adiabatic electron affinities (EA_{ad}) range from 1 to 2 eV. The vertical detachment energies are between 1.3 and 4.0 eV. The adiabatic ionisation energies (IE_{ad}) are in the 9.9–10.2 eV range. The vertical ionisation energies are in the 10.4–10.9 eV range. It is shown that NO_2^-/NO_2 loss would be common in anions and cations, respectively. Isomerisation and N—N bond dissociation accompany cation and anion formation, respectively. The suggested mass spectral fragmentation products for the cations along the S_0 surface are 84, 130, and 176 amu, in agreement with earlier mass spectrometry studies.

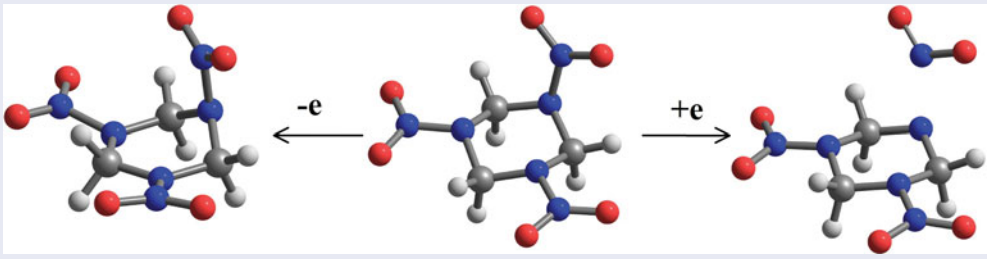

ARTICLE HISTORY
Received 20 July 2016
Accepted 3 October 2016

KEYWORDS
RDX; DFT; dissociation mechanism; ion; mass spectrometry

Introduction

Laser desorption-ionisation (LDI) is considered a candidate for *in situ* detection of low volatility energetic compounds such as 1,3,5-trinitro-1,3,5-triazacyclohexane (RDX) [1] present on *any* surface. In LDI, the molecules on the surface of a bulk are brought to the gas phase predominantly as a neutral plume by laser desorption. The molecules in the plume are subsequently ionised by a second laser pulse and are typically detected by a mass spectrometer. For selective detection, a molecule strictly specific to RDX should be produced as a marker.

Energetic molecules like RDX are a great challenge for LDI because they decompose below their melting point upon heat treatment and they also decompose readily in a mass spectrometer upon ionisation. In order to use a method like LDI on RDX detection, it is necessary to minimise thermal decomposition at the initial ablation step to generate intact RDX(g) and to enhance the production of the marker from the RDX(g) by controlling the laser-ionisation process. Bernstein *et al.* were able to desorb intact RDX by matrix assisted laser desorption and subsequent supersonic jet expansion [2–4]. In this way, neutral RDX beam could be produced by ablation. However its excited state decomposition was investigated through the use of NO/NO^+ by mass spectrometry, rather than RDX^+.

Earlier work on RDX focused on energetic and molecular aspects of thermal decomposition of RDX in the gas and condensed phases and used mass spectrometry for detection of the decomposition products [5–13]. These mass spectrometry and optical spectroscopy studies showed that contributions of thermal decomposition and mass spectral decomposition pathways to the mass spectra were not the same [9]. With the internal energy gained during ionisation, mass spectral fragmentation of RDX^+ was suggested to proceed by several mechanisms such as N–N bond fission, $CH_2N_2O_2$ elimination followed by ring contraction, and ring fragmentation [9].

CONTACT F. A. Akin ahu.akin@boun.edu.tr
Supplemental data for this article can be accessed at http://dx.doi.org/10.1080/00268976.2016.1246759.

The calculated N–N bond order in the excited state RDX^+ was found to be lower than that in the ground state RDX^+. It was, therefore, suggested that mass spectral decomposition should occur from the excited state of RDX^+ rather than the ground state [6,11]. In a chemical ionisation source, RDX formed adducts with NO and NO_2. Mass spectral decomposition of these ions was observed along with that of RDX^+ [9]. The molecular ion, $[RDX]^+$, was not abundant in the mass spectra.

The ground state global minimum of RDX molecule is experimentally reported to have C_3 symmetry with $-NO_2$ groups in axial positions over a 1,3,5-triazacyclohexane ring with chair conformation. Further computational studies of RDX decomposition used this structure as the starting point [14]. In LDI, ablation can produce conformers other than the one the molecule adopts on the surface or the analyte can be locked into a less stable conformation, the kinetically favoured product, during expansion into vacuum [15–17]. Different conformers of RDX are defined by different combinations of the axial-equatorial position of the $-NO_2$ groups and various (chair, boat, and twisted-chair) conformations of the heterocyclic ring system. Upon ionisation of these RDX conformers, conformational effects on the vibrational modes excited would have an impact on which unimolecular dissociation pathway is preferred by the ground state RDX^+.

During ablation of a molecule from a metal surface it is possible to produce electrons and negative ions [18]. Therefore, depending on the surface, formation of RDX^- is possible even during ablation (prior to laser ionisation). In a variant of LDI, laser desorption electron attachment time-of-flight mass spectrometry, negative ions are created from the neutral ablation plume by low energy electron attachment and are used in the detection of non-volatile compounds [19]. The fate of RDX^- created by the processes described above is unknown to our current knowledge. Therefore, in addition to cation formation, formation of RDX^- and its possible fragmentation pathways should also be of interest.

In this work, the fate of the neutral structures upon electron attachment and ionisation was discussed by structural comparison between the neutral and charged RDX. Structures, ionisation energies (IE), and electron affinities (EA) of RDX conformers are reported. Rather than ionisation of the hot RDX, we focus on the ionisation of the surviving neutrals at room temperature.

Method

Geometry optimisations

We found five isomers of RDX within 1 kcal/mol of each other, four of which are stable at all levels of theory employed and will be the subject of this study. The AAA-*chair* (C_{3v}) isomer was taken from Goddard's work [14,20]. RDX has a similar C_3 conformation in the β crystalline form and in the gas phase [21]. Three low energy isomers were isolated by molecular mechanics using Tork method [22]. The four isomers are the AAA-*chair* (C_{3v}), AAE-*chair* (C_s), EEA-*chair* (C_s), and the EAA-*twisted boat* (C_1) conformers. The AAE-*chair* (C_s) conformation is the conformation RDX adopts in crystalline α form [23].

The neutrals were optimised at the B3LYP/6-31+G(d,p) level [24]. Minima were confirmed via frequency calculations. Tight SCF convergence criteria were employed for the optimisations and frequency calculations. Neutral geometries from B3LYP/6-31+G(d,p) calculations were further optimised using MPW1B95/MG3S [25,26] to check for consistency of the geometries and to obtain superior energies needed for IE calculations. Similarly, the neutrals were also optimised and frequency-checked at the B98/MG3S [27] level for further calculation of their EA.

The neutral species have closed shell wavefunctions. Ions were open-shell with doublet spin states. None of the structures presented in this work showed severe spin contamination, 'S^2' values were between 0.75 and 0.77.

The difference of the calculated final ion geometries from the neutral starting geometries are dependent on the optimisation step size employed. The cation/anion at the neutral geometry is not necessarily a transition state but a higher order saddle point. IRC calculations are therefore not always feasible for proof of shortest connection path between the neutral and its anion/cation. A more detailed study in which step size is treated as a variable and the proximity in the geometries of the neutral and ionic RDX is set as the primary criterion may be carried out in the future. It is also possible to include higher energy RDX neutrals which may lead to low energy cation isomers. Finally, possibility of connections between every neutral isomer and every anion/cation could be assumed and explored. The scope of this study is limited to **(1)** answering whether the anion/cation will be stable within the neutral geometry, (2) finding the ion structures using methods that can reproduce experimental geometries for the neutrals, and (3) establishing a connection between the results of calculated neutral→ion transitions and the experimental fragmentation patterns.

Ionisation energies

The cations were prepared by removing an electron from the highest unoccupied molecular orbital (HOMO) of the neutrals and were doublet cations. They were optimised at the B3LYP/6-31+G(d,p) and MPW1B95/MG3S

levels. The adiabatic ionisation potential is calculated using Equation (1), where M^+ indicates cation at its optimised ground state geometry, M indicates neutral at its optimised ground-state geometry, T_0 is the electronic energy, and ZPE is the zero-point energy:

$$\mathrm{IE_{ad}} = (T_0 + \mathrm{ZPE})_{\mathrm{M+}} - (T_0 + \mathrm{ZPE})_{\mathrm{M}} \quad (1)$$

The vertical ionisation energies (VIE) are calculated by the following where M^+(R:M) indicates cation at the neutral geometry. Since it is not at a minimum on the cation potential energy surface, negative frequencies emerge during normal mode analysis. These modes were excluded from the ZPE calculation:

$$\mathrm{VIE} = (T_0 + \mathrm{ZPE})_{\mathrm{M+(R:M)}} - (T_0 + \mathrm{ZPE})_{\mathrm{M}} \quad (2)$$

Vertical and adiabatic ionisation energies were calculated by single point calculations at the B3LYP/Aug-cc-pVXZ (X = T,Q) level on B3LYP/6-31+G(d,p) geometries as well as at the MPW1B95/MG3S level on the MPW1B95/MG3S geometries. The MPW1B95/MG3S method has a mean unsigned error (MUE) of 0.09 eV in IE.

Electron affinities

The anions were prepared by adding an electron to the lowest unoccupied molecular orbital (LUMO) of the neutrals. The structures were optimised at the B3LYP/6-31+G(d,p) and B98/MG3S levels. The adiabatic electron affinities were calculated using Equation (3) below. The M^- indicates anion at its optimised ground-state geometry:

$$\mathrm{EA_{ad}} = (T_0 + \mathrm{ZPE})_{\mathrm{M}} - (T_0 + \mathrm{ZPE})_{\mathrm{M-}} \quad (3)$$

To calculate the vertical detachment energies (VDE), M^- was replaced by M(R:M^-), namely the neutral at anion geometry:

$$\mathrm{VDE} = (T_0 + \mathrm{ZPE})_{\mathrm{M(R:M-)}} - (T_0 + \mathrm{ZPE})_{M-} \quad (4)$$

EA and VDE were calculated by single point calculations at the B3LYP/Aug-cc-pVXZ (X = T,Q) level on B3LYP/6-31+G(d,p) geometries. They were also calculated at the B98/MG3S level using the B98/MG3S geometries. The B98/MG3S has an MUE of 0.08 eV [25] in EA.

All calculations were carried out using Gaussian 03 software [28].

Results and discussion

Neutral geometries

It is well known today that the charge-transfer centres are the $-NO_2$ groups around the ring system of RDX. The heterocyclic ring also has an important role in the fragmentation processes. A computational method which can simulate the electronic environment around both the $-NO_2$ functional group and the heterocyclic ring system of RDX should be used. Calculations on molecules similar to RDX, namely those in the form of R–NO_2 whose experimental geometries are available were carried out and the calculated geometries and ionisation/photodetachment energetics were compared to the available experimental values. Specifically, we optimised the geometries of ground state $NO_2(^2A_1)$, $NO_2^+(^1A_1)$, and $NO_2^-(^1A_1)$ and calculated the IE and EA of similar small organic molecules (N_2O_4, CH_3NO_2, and $(CH_3)_2NNO_2$). The results were checked against the literature experimental [29–37] and computational [38–40] studies. The results are reported wherever relevant, and they support our choice of basis sets and methods.

The optimised structures of the four isomers (AAA-*chair* (C_{3v}), AAE-*chair* (C_s), EEA- *chair* (C_s), and the EAA-*twisted boat* (C_1) conformers) and their short designations (IV, I, II, and III, respectively), are given in Figure 1. All isomers are in their totally symmetric singlet states ($^1A_1$, 1A', 1A', and 1A, respectively). Table 1 shows the relative energies of the isomers calculated by each method used in this study. All methods except for MPW1B95/MG3S predict that the AAE-*chair* (C_s) is the lowest energy conformer among the four structures. The calculations using the MPW1B95/MG3S method predict that the EAA-*twisted boat* (C_1) is the minimum energy conformer. The experimentally relevant gas phase structure of the AAA-*chair* (C_{3v}) conformer appears to be of higher energy. All isomers fall within a 5 kJ/mol interval. Bond distances, bond angles and torsional angles are given in Table S1 and Table S2 in the supplemental data in comparison with the experimental results of Shishkov *et al.* [20].

The B3LYP/6-31+G(d,p) method simulates the free NO_2 ground state geometry well: the calculated r_{NO} = 1.202 Å and α_{ONO} = 134.0°, whereas the experimental values are 1.194 Å and 133.9°, respectively [41]. The B3LYP/6-31+G(d,p) geometry for $(CH_3)_2NNO_2$ is also in good agreement with experimental values for this molecule [42]; the calculated CN and NN bond distances and the CNN angle are within the experimental range defined by the uncertainties. The calculated NO bond distance is outside the error margins only by 0.01 Å, and the ONO and CNC bond angles are smaller than the

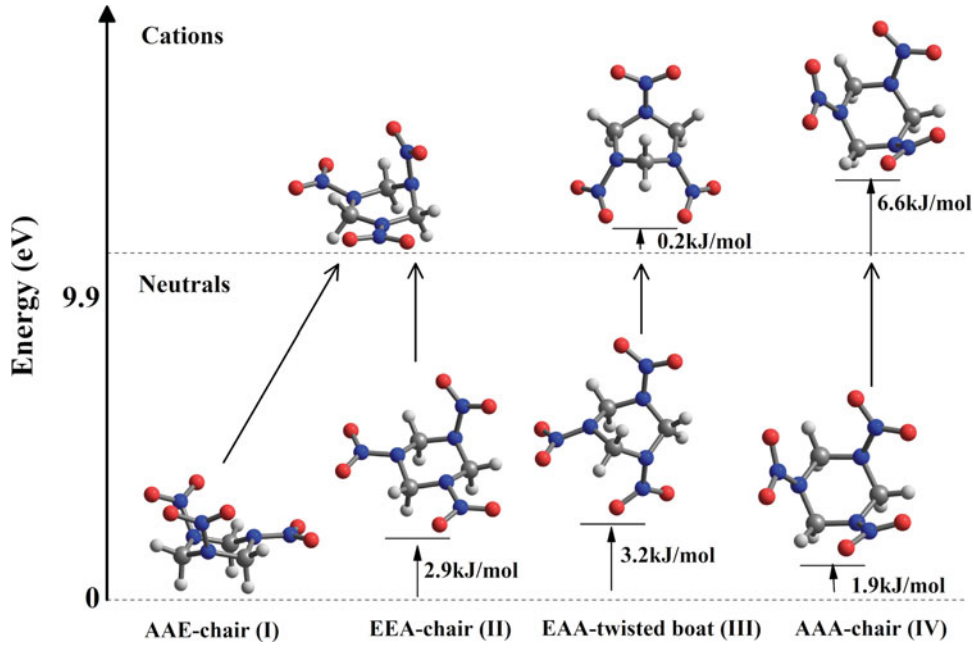

Figure 1. The structures of RDX neutrals and cations are shown. The structures have been optimised at the B3LYP/6-31+G(d,p) level of theory and the energies are calculated at the B3LYP/Aug-cc-pVTZ level. The B3LYP energies are the sum of electronic energy (Aug-cc-pVTZ) and the zero point energy (6-31+G(d,p)). The dashed lines indicate the location of the lowest energy conformer at the corresponding charge state.

experimental values by 3% and 5%, respectively. According to the experimental results, concerning NO_2 and $(CH_3)_2NNO_2$, when NO_2 is attached to a nitrogen with alkyl groups, the NO bond is slightly stretched from 1.193 to 1.223 Å and the ONO angle decreases from 134.1° to 130.4°. When the two $-CH_3$ groups are replaced by a $-CH_2-N(NO_2)-CH_2-$ heterocyclic ring system as in RDX, the N–O bond shrinks slightly (from 1.223 to 1.213 Å) and the ONO angle becomes more acute (from 130.4° decreases to 125.5°). Going from NO_2 to RDX (C_{3v}), the computational results mimic this trend, the N–O bond is stretched from 1.202 to 1.224 Å and the ONO angle is reduced (from 134.0° to 126.8°). The 6-31+(d,p) basis set is adequate to describe the electronic environment around the neutral structures. The results for the AAA-*chair* C_{3v} conformer agree well with Goddard's 6-31G(d) structure. To be able to use a unified methodology for anions as well as the neutrals and the cations, the 6-31+(d,p) basis set was chosen instead of 6-31G(d).

In all neutral conformers, the N–O, N–N, and C–N bond lengths cover a range of 1.221–1.231, 1.389–1.436, and 1.451–1.480 Å, respectively. In all conformers except the C_{3v} conformer, all axial C–H bonds are longer (1.089–1.104 Å) than the equatorial C–H bonds (1.084–1.089 Å). The N–N bonds involving the $-NO_2$ groups in the equatorial position are shorter. Also the C–N bonds involving the ring N atoms to which these $-NO_2$ groups are connected are longer. The equatorial positioning brings about a weakness to the ring in these locations.

Cations

Upon removal of an electron from the neutral geometries and after full geometry optimisation, the cation structures in Figure 1 are found, with structural parameters listed in Table S2 in the supplemental data.

The EEA-*chair* and AAE-*chair* structures of C_s symmetry converged to the same cation. Conversion from the chair structure to the boat structure is the most striking

Table 1. Relative energies of RDX neutrals, anions and cations in kJ/mol. In each set, the lowest energy species is taken as the reference. For cases in which the energies are the same, the actual values are provided in parentheses.

	Relative energies (kJ/mol)						
	B3LYP/TZ//B3LYP/6-31+G(d,p)			B98/MG3S		MPW1B95/MG3S	
	Neutral	*Anion*	Cation	Neutral	*Anion*	Neutral	Cation
AAE-*chair* (C_s)	0	*50*	0	0	44	1	20
AAA-*chair* (C_{3v})	2	*65*	7	1	74	4(3.8)	14
EEA-*chair* (C_s)	3(2.9)	*9*	0	4	10	4	1
EAA-*twisted boat* (C_1)	3(3.2)	*0*	0 (0.2)	3	0	0	0

change that occurs upon cationisation. The C_s symmetry is preserved. The other major changes occur around the –NO_2 groups and the ring C–N–C bonds. The N–N bonds stretch while the N–O bonds shrink and all O–N–O angles increase. (The NO_2 cation is linear with rNO = 1.129 Å.) The ring N–C–N and the C–N–C angles increase by 7.5° and 6.7°, respectively.

Removal of an electron from the AAA-*chair* (C_{3v}) conformer causes a drop in symmetry from C_{3v} to C_s due to a substantial increase in two of the N–N bond lengths from 1.418 to 1.533 Å. All O–N–O bond angles in these two –NO_2 groups increase by 5.7° and reach 132.5°, very close to the O–N–O angle in the neutral molecular NO_2 ground state (rNO = 1.202 Å and α_{ONO} = 134.0° per the B3LYP/6-31+(d,p) method). The N–O bond lengths decrease from 1.224 to 1.201–1.204, again resembling the N–O bond lengths in the neutral molecular NO_2 ground state. The N–C–N angle involving the C atom across the axial –NO_2 decreases substantially by 10.6°. The ring conformation does not change.

Finally, removal of an electron from the EAA-*twisted boat* (C_1) conformer results in a cation of higher symmetry (C_s). The N—N bond lengths increase substantially from around 1.4 to 1.5 Å. All the N–O bond lengths decrease. There is a decrease in the ring C–N bond lengths on average.

While all N–N bond lengths increase, two of the three N–N bonds are stretched more than the third regardless of whether the –NO_2 groups connected by these N–N bonds are in axial or equatorial positions. The amount of N–N extension is higher in the cationisation of the AAA-*chair* (C_{3v}) conformer and the almost detached -NO_2 groups resemble the neutral molecular NO_2 ground state geometry. The resemblance is pronounced in this conformer more than the others; cationisation pushes the –NO_2 groups farthest from the ring (1.533 Å). During cationisation, resemblance of the –NO_2 groups to neutral molecular –NO_2 is inversely correlated with the N–N bond strength. Therefore, a picture with neutral NO_2-cationic ring complex emerges. The results of charge analysis of the cations (see Table S3 in the supplemental data) indicate that ≥ 65% of the positive charge remains on the ring atoms. Each -NO_2 group carries a very small partial positive charge of +0.1. This suggests that when an electron is removed from RDX, cationisation could proceed with an obvious loss of neutral –NO_2 groups which are ionised and detected in the later stages of ionisation (via charge-transfer or during multi-photon absorption).

Anions

Upon addition of an electron to the neutral geometries and after full geometry optimisation, the anion structures in Figure 2 are found, with structural parameters listed in Table S2 in the supplemental data.

Addition of an electron to both the EEA-*chair* (C_s) and the EAA-*twisted boat* (C_1) conformers causes one of the –NO_2 groups to be detached: the –N···NO_2 distances are 2.24 and 2.31 Å, respectively. The detached –NO_2 group has the geometry (r = 1.235 Å, α = 124°) in the former and (r = 1.240Å, α = 123°) in the latter. This geometry is in the midpoint between the calculated ground state geometries of NO_2 ($X\,^2A_1$, α = 134.0°, r = 1.202 Å) and NO_2^- ($X\,^1A_1$, α = 116.5°, r = 1.264 Å). The CHELPG charge analysis (B3LYP/Aug-cc-pVTZ) of the EEA-*chair* (C_s) indicates that the detached –NO_2 group carries half the negative charge of the anion amounting to −0.4 ē (δ_N = +0.4, both O atoms δ_O = −0.4). The situation is similar for the detached –NO_2 group in EAA-*twisted boat* (C_1): the detached –NO_2 group carries 45% of the negative charge in this isomer. This causes repulsion of the –NO_2 group from the ring. Owing to the small positive charge on the N atom of the detached –NO_2 group, the ring keeps the –NO_2 group close.

In response to the detachment of the axial –NO_2 group, the C–N bonds of the ring undergo substantial changes in the EEA-*chair* (C_s) conformer. The C–N bond distances shrink considerably (from 1.451 to 1.408 Å) in the –CH_2–N–CH_2– moiety left behind after the expulsion of the axial –NO_2. This moiety distances itself from the rest of the molecule (–N(NO_2eq)–CH_2–(NO_2eq)N–) by extension of the C–N (from 1.474 to 1.512 Å) bonds connecting these two parts. The EAA-*twisted boat* (C_1) conformer shows similar changes as the EEA-*chair* (C_s) conformer. The C–N bond lengths in the –CH_2–N–CH_2– and (–N(NO_2eq)–CH_2–(NO_2ax)N–) moieties decrease making each group more compact. In addition, the ring conformation is no longer a twisted-boat but is rather in a proper boat conformation. These changes show that in these anions of RDX, loss of the –NO_2 groups activates the vibrations in the remaining ring and could initiate ring fission. This issue will be addressed in a subsequent publication.

The remaining isomers, namely, the AAE-*chair* (C_s) and the AAA-*chair* (C_{3v}) retain their symmetry and bonding pattern during optimisation from the neutral to the anionic state. The change in bond lengths and angles are modest. The N—O bonds are longer and the N—C—N bond angle is slightly (2.3°) wider in both anions. The N–N–C bond angle is more acute by 2.9 in the AAE-*chair* anion.

The charge-dipole anion complexes of the EAA-*twisted boat* (C_1) and the EEA-*chair* (C_s) are more stable than the intact AAE-*chair* (C_s) and the AAA-*chair* (C_{3v}) conformers. The relative energies of the anions are given in Table 1. The EAA-*twisted boat* (C_1) conformer

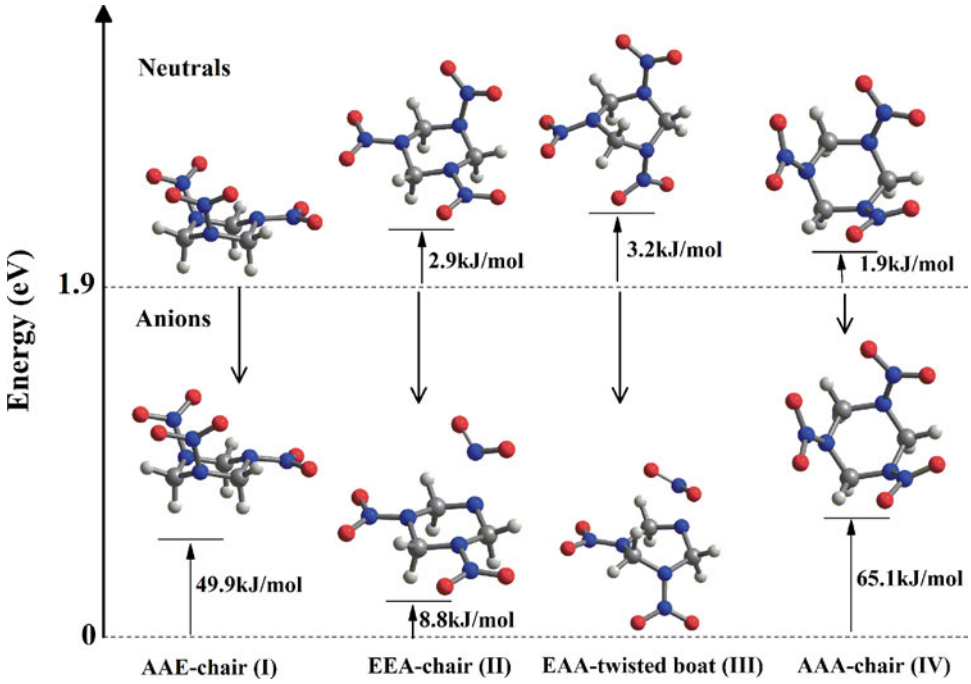

Figure 2. The structures of RDX neutrals and anions are shown. The structures have been optimised at the B3LYP/6-31+G(d,p) level of theory and the energies are calculated at the B3LYP/Aug-cc-pVTZ level. The B3LYP energies are the sum of electronic energy (Aug-cc-pVTZ) and the zero point energy (6-31+G(d,p)). The dashed lines indicate the location of the lowest energy conformer at the corresponding charge state.

is the most stable anion and it is more stable than the EEA-chair (C_s) conformer by 8–10 kJ/mol. The AAE-*chair* (C_s) and the AAA-*chair* (C_{3v}) conformers are 44 and 74 kJ/mol higher than the EAA-*twisted boat* (C_1) conformer, as per the B98/MG3S energies. According to the B3LYP/6-31+G(d,p) PES (Figure 3) for both the EAA-*twisted boat* (C_1) and the EEA-*chair* (C_s) conformers the complex has a well depth of 0.4 eV (0.3 after BSSE correction) for the N–N bond dissociation coordinate. The MMUE [25] for D_e for species with weak interactions is 0.32 kcal/mol (0.014 eV) with or without BSSE corrections.

Ionisation energies and electron affinities

Table 2 shows the vertical and adiabatic ionisation energies of the four conformers calculated using various DFT functionals and basis sets. The experimentally available energy quantities for NO_2, N_2O_4, CH_3NO_2, and $(CH_3)_2NNO_2$ are calculated and comparison between the calculated and experimental values [35–36] are shown. The B3LYP/TZ//B3LYP/6-31+G(d,p) and the B3LYP/QZ//B3LYP/6-31+G(d,p) yield similar energetics within the eV scale. The MPW1B95/MG3S method produces better ionisation potentials than those obtained by the B3LYP functional. The MUE for ionisation potentials calculated by the MPW1B95/MG3S method (for QCISD/MG3 geometries) is 2.14 kcal/mol (0.09 eV) [25]. The calculated adiabatic ionisation potential (IP) values for NO_2, N_2O_4, CH_3NO_2, and $(CH_3)_2NNO_2$ are consistent with the experimental values within the same MUE even though the geometries have been calculated using the MPW1B95/MG3S method rather than the QCISD/MG3. All adiabatic IP values are within 9–11 eV range, and the vertical IP values are within 10.4–11.5 eV range.

Table 3 shows the VDE and the adiabatic electron affinities of the four conformers calculated using various DFT functionals and basis sets. The experimentally available energy quantities for NO_2 are calculated and comparison between the calculated and experimental values are shown. The agreement between the experimental and the B98/MG3S EA of NO_2 is within 0.08–0.09 eV for both the vertical and adiabatic cases. This difference is within the MUE for EA calculated by B98/MG3S method which is 0.08 eV (1.84 kcal/mol) for QCISD/MG3 geometries [25]. The RDX conformers have lower EA than NO_2 [43].

There is a large difference between the vertical detachment energy and the adiabatic electron affinity of the EEA-*chair* (C_s) and those of the EAA-*twisted boat* (C_1) conformer. These anions are not stable in the neutral structural forms but rather as charge-dipole complexes in which the N–N bond is broken (Fig. 2). The vertical detachment energy of these anions is large because the neutral with the broken N–N bond is unstable.

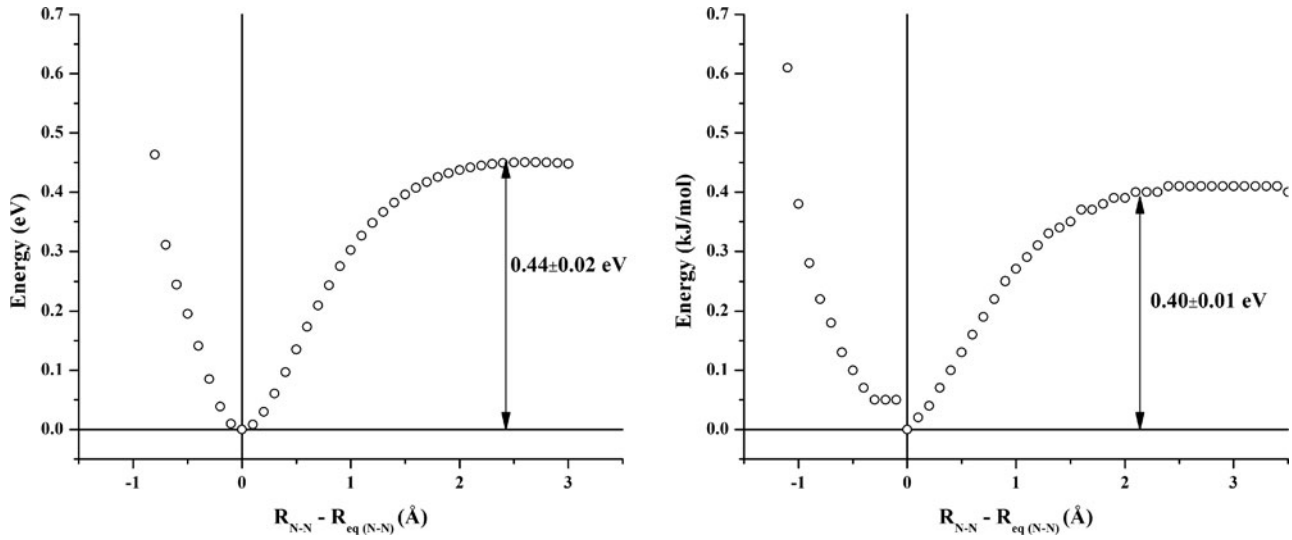

Figure 3. The potential energy diagrams for N–N dissociation coordinate in EEA-*chair* (left), and EAA-*twisted boat* (right) anions. The values for binding energy are the average of all points at the plateau region [after r (N–N) = 2 Å] with ±standard deviation. The inflection point at the left of the $x = 0$ line for the EAA-*twisted boat* anion (right) is due to favourable (O–N–)O …H(C) interactions in the repulsive side of the potential. There is a basis set superposition error of 0.1 eV at the minimum of the potentials, bringing the binding energies to ∼0.3 eV range.

Since the gap between these two quantities are too large, experimental observation of either quantity would be difficult even if the original anion charge-dipole complexes survived from production until detection.

The connectivity in the anion and neutral of the AAE-*chair* (C_s) are similar. In addition, the structural parameters of the anion and the neutral are similar. Consequently, there is little difference between the VDE and

Table 2. IE of the RDX isomers and relevant nitro compounds with available experimental values are given. The experimental values are given in parentheses, from Ref. [35].

	IE (eV)					
	B3LYP/TZ//B3LYP/6-31+G(d,p)		B3LYP/QZ//B3LYP/6-31+G(d,p)		MPW1B95/MG3S	
	VIE[a]	IE_{ad}[b]	VIE	IE_{ad}	VIE	IE_{ad}
AAE-*chair* (C_s)	10.5	9.9	10.4	9.9	10.9	10.2
AAA-*chair* (C_{3v})	10.2	10.0	10.2	10.0	10.4	10.1
EEA-*chair* (C_s)	10.5	9.9	10.5	9.9	10.5	9.9
EAA-*twisted boat* (C_1)	10.2	9.8	10.2	9.9	10.4	10.0
NO_2	11.8	9.9	11.8	9.9	11.5 (11.23)	9.6(5) (9.586)
N_2O_4	11.5	10.2	11.5	10.2	11.5 (11.4)	10.1 (10.8)
CH_3NO_2	–	11.0	–	11.0	–	11.0 (11.08±0.04)
$(CH_3)_2NNO_2$	9.9	9.3	9.8	9.3	9.8(N/A)	9.4 (9.53)

[a] Vertical ionisation energy. [b] Adiabatic ionisation energy.

Table 3. EA of the RDX isomers and NO_2 are given. The experimental values for NO_2 are given in parentheses.

	EA (eV)					
	B3LYP/TZ//B3LYP/6-31+G(d,p)		B3LYP/QZ//B3LYP/6-31+G(d,p)		B98/MG3S	
	VDE[a]	EA_{ad}[b]	VDE	EA_{ad}	VDE	EA_{ad}
AAE-*chair* (C_s)	1.8	1.4	1.8	1.4	1.7	1.3
AAA-*chair* (C_{3v})	1.5	1.3	1.5	1.3	1.3	1.1
EEA-*chair* (C_s)	3.8	1.9	3.8	1.8	3.7	1.7
EAA-*twisted boat* (C_1)	4.1	2.0	4.1	1.9	4.0	1.8
NO_2	2.92	2.25	2.92	2.24	2.78 (2.66)[c]	2.16 (2.25)[d]

[a] Vertical detachment energy. [b] Adiabatic electron affinity. [c] Ref. [39]. [d] Ref. [43].

EA values. The anion and the neutral of the AAA-*chair* (C_{3v}) conformer have a similar relationship which yields similar VDE and EA values for this species.

Comparison between proposed and experimental dissociation pathways

The proposed fragmentation pathways of the RDX isomer anion and cations are shown in Table 4. The neutral RDX conformer HOMOs have major contribution of ring nitrogen 2p orbitals and minor contribution of the $-NO_2$ nitrogen 2p orbitals in antibonding configuration. Electron attachment adds the electrons onto the $-NO_2$ groups and diminishes the contribution of ring nitrogens to the new HOMO (Figure S1). This removes the *valence* atomic orbital interactions partially responsible for ring strain. For this reason, boat→chair conversions are not encountered in anion formation. However, $-NO_2$ loss leads to changes in the bond structure of the ring, stimulating fragmentation.

The EEA-*chair* and EAA-*twisted-boat* anions showcase prompt $-NO_2$ loss upon electron attachment. The CHELPG analysis of the charges on the three $-NO_2$ groups in the anions and cations of all isomers show that (see Table S3 in the supplemental data) (1) the −1 charge is almost entirely on the NO_2 groups in all anions and (2) the EEA-*chair* and EAA-*twisted-boat* anions have the detached NO_2 take half the charge load. This rules out the neutral excited states for the detached NO_2. Relaxed potential energy scans along the extended N–N coordinate (with symmetry restrictions removed) yielded detached NO_2 group geometries $r = 1.235$ Å and $\alpha = 124°$ (EEA-*chair*) and $r = 1.240$ Å, $\alpha = 123°$ (EAA-*twisted-boat)*. For the EAA-*twisted-boat* anion, the NO_2 r and α values started at $r = 1.240$ Å and $\alpha = 123°$, then formed a plateau at $r = 1.229$ Å and $\alpha = 124.9°$ at a distance of 6.9 Å. Similar results were obtained for the EEA-*chair*. Keeping NO_2 at $r = 1.229$ Å and $\alpha = 124.9°$, vibrational frequencies were calculated for the X^1A_1 and $^3B_1$ states (lowest energy triplet) of NO_2^-. For both states, this geometry produced positive vibrational frequencies, i.e. is a minimum. The HOMO of the EEA-*chair* and EAA-*twisted-boat* anions have contributions from the HOMO of the detached NO_2 ($6a_1$ orbital) and a p orbital on the ring nitrogen aligned with the N–N bond axis in an antibonding configuration. The intact AAE-*chair* and AAA-*chair* anion HOMOs are composed entirely from the NO_2 HOMOs. The potential energy surface for $[RDX]^- \rightarrow [RDX\text{-}NO_2] + NO_2^-$ pathway has to be studied using methods that can treat excited states properly, exemplified by Bernstein and Bhattacharya [44], Arenas *et al.* [45], Florián *et al.* [46], and Jeilani *et al.* [47].

The cases of AAE-*chair* and AAA-*chair* anions are different because there is no preferred $-NO_2$ group that is chosen to carry the negative charge. For the AAA-*chair*, the (−1) charge is partitioned such that all $-NO_2$ groups have most of the charge, a total of -0.67 electron, equally partitioned. The anion HOMO contributions are equivalent for all $-NO_2$ groups. The potential energy surface for this *complex* coordinate should be explored further however, we can speculate that the ring system will remain neutral and one $-NO_2$ group could carry the charge.

In the AAE-*chair*, the equatorial $-NO_2$ is the preferred negative charge center (−0.329 vs −0.284 electron). This results in several possibilities: one where the charge remains on the ring system with departure of two neutral NO_2 groups, one where the charge is carried away on the departing equatorial NO_2 group, or the equatorial NO_2 group departs as a neutral, leaving behind a charged fragment anion.

From our calculations, the common theme in RDX anion dissociation is the observation of 46 (NO_2^-) amu/ē from all isomers. In the case of the ion–dipole complexes, since the electron affinity values are higher than the potential well for NO_2^- expulsion, the energy output upon electron attachment will cause prompt NO_2^- loss. Negative ion chemical ionization (NCI) spectra of Yinon *et al.* [9] produced 46 (NO_2^-), 84 ($C_2H_2N_3O^-$), 130 ($C_3H_6N_4O_2^-$), and 176 ($C_3H_6N_5O_4^-$) amu/ē ions from both RDX and HMX via resonance and dissociative electron capture. Experimental work on anions similar to RDX have also proceeded via NO_2^- loss [46–48]. In their experiments, Yinon *et al.* [9] report the precursor to be the $[RDX+NO_2]^-$ ion. The 129, 130, and 176 amu/ē ions are first generation daughter ions as also shown in this work. The 84 amu/ē fragment is a second generation anion born of 129 ($C_3H_5N_4O_2^-$) amu/ē precursor. There is a difference in the experimental structural assignment of the 84 amu/ē fragment ($C_2H_2N_3O^-$) by Yinon *et al.* and our proposed ($C_3H_6N_3^-$) structure. Production of $C_3H_6N_3^-$ would also require more energy for it to be observed as a first generation daughter ion in NCI experiments.

For the cationic isomers, the picture is reversed, i.e. most of the positive charge is on the ring system. Also, three out of four of the RDX isomers go through alteration in the ring conformation upon becoming a cation, i.e. cationisation destabilises the chair conformation. All conformer HOMOs have ring nitrogen 2p contributions and electron removal does not change the orbital picture. The ring nitrogen and $-NO_2$ 2p orbitals are arranged in antibonding fashion which contributes to the ring strain. These factors cause (1) an increased number of dissociation pathways and (2) more ring dissociation pathways to emerge.

Table 4. The expected initial dissociation products based on visible changes in the anion and cation geometries. When more than one ionic product is possible, in order to save space, the products' molecular formulae are augmented with the '$-\delta\forall$ (or' $+\delta\forall$) superscript. The δ is equal to a full (not partial) charge of 1 in each case so only one of the products can be assigned the charge. For cases where two '$-\delta\forall$ (or' $+\delta\forall$) designations are used, it means there are two possible product channels producing either one or the other ionic product, and the rest of the products are neutral.

	Proposed MS fragmentation pathway	
Name	$M^- \rightarrow$	$M^+ \rightarrow$
AAE-*chair*	$[M-2NO_2]^-$ (130 amu) + $2NO_2$ $[M-NO_2]\delta$ (176 amu) + $NO_2{}^-\delta$ (46 amu)	$[M-NO_2]^+$ (176 amu) + NO_2
AAA-*chair*	$[M-3NO_2]$ + $NO_2{}^-$ (46 amu) + $2NO_2$ $[M-3NO_2]^-$ (84 amu) + $3NO_2$	$[M-NO_2]^+$ (176 amu) + NO_2 $[M-2NO_2]^+$ (130 amu) + $2NO_2$ $[M-3NO_2]^+$ (84 amu) + $3NO_2$
EEA-*chair* EAA-*twisted boat*	$[M-NO_2]^{-\delta}$(176 amu) + $NO_2{}^-$ (46 amu) $[M-NO_2]$ + $NO_2{}^-$ (46 amu)	$[M-2NO_2]^+$(130 amu) + $2NO_2$ $[M-NO_2]^+$ (176 amu) + NO_2 $[M-2NO_2]^+$ (130 amu) + $2NO_2$ $[M-3NO_2]^+$ (84 amu) + $3NO_2$

In RDX cations, the CHELPG charges do not exceed 0.13 for any of the $-NO_2$ groups. The N–N bond distances are longer than their neutral and anionic counterparts. Therefore, based on the initial state of the $-NO_2$ groups, a picture where expulsion of neutral $-NO_2$ leaving behind a cation emerges. All $-NO_2$ group geometries are very similar to the neutral free NO_2 geometry.

The predicted first generation daughter ions are the NO_2 loss channels, m/z 84 ($C_3H_6N_3^+$), 130 ($C_3H_6N_4O_2^+$), and 176 ($C_3H_6N_5O_4^+$). Producing these ions would require the least energy. Mass spectrometry studies of Yinon [9], Stals *et al.* [6], Snyder *et al.* [11], Shannon *et al.* [12] and Farber *et al.* [7] used different ionisation methods prior to mass analysis. The results support the mechanisms revealed by Yinon *et al.* for the production of m/z 176 (neutral NO_2 loss). In their CI/CID spectrum, m/z 131 $[130 + H]^+$ has a dominant contribution from the $C_3H_7N_4O_2^+$ ($[M\text{-}2NO_2 + H]^+$) ion, in agreement with our calculations. Concerning neutral NO_2 loss, as mentioned by the authors [9], CHELPG results are in dispute with Bulusu *et al.* [5] whose proposed fragmentation mechanisms involved direct production of NO_2^+ from RDX. Stals *et al.* [6] and Snyder *et al.* [11] report m/z 84 and 85 ions, respectively. While there is agreement between present work and the results of Stals *et al.* [6] on the structure of the m/z 84 ion, the m/z 85 ion observed in the pyrolysis-atmospheric pressure CI studies of Snyder *et al.* [11] is not the same as proposed by present calculations. Snyder *et al.* proposed that the chemical formula for m/z 85 ion is $C_4H_9N_2^+$. Snyder *et al.* attributed the difference to the differences in ion production; $C_3H_7N_3^+$ was produced by ionisation of intact gaseous RDX but Py-APCI involved ionisation of thermal decomposition products of RDX.

Conclusion

The four well-known neutral RDX isomers, AAE-*chair*, AAA-*chair*, EEA-*chair*, and EAA-*twisted boat*, are found to exist within a 4 kJ/mol energy interval at B3LYP/6-31+G(d,p) level. Consequently, a minimum of four isomers could coexist in a neutral RDX beam at room temperature prior to ionisation for mass analysis.

The RDX neutral conformers have lower EA than NO_2 but they could become anionic, with EA_{ad} values ranging from 1 to 2 eV. The formation of charge-dipole complexes in the anions increases the VDE to as high as 3.7, 4.0 eV in two isomers, making RDX less amenable for photodetachment spectroscopy. The IE_{ad} values are in the narrow 9.9–10.2 eV range, similar to other nitro-compounds. Due to isomerisation upon electron loss, the VIE are higher, in the 10.4–10.9 eV range.

Based on geometric changes alone, each RDX isomer fragmentation supports earlier experimental results in that, in anions NO_2^- loss, in cations NO_2 loss is common. In anions, $-NO_2$ groups either detach as NO_2^- and form charge–dipole complex (of 0.3-0.4 eV well-depth) with the ring or remain in the RDX structure but share the negative charge. In cations, the N–N bonds are weaker than they are in neutral RDX and the $-NO_2$ group geometries are close to that of neutral free NO_2. Therefore, electron loss would result in loss of one or more $-NO_2$ groups. A study that delves into more inconspicuous mechanisms leading to ring dissociations in RDX due to electron density shifts and vibrational activation is completed and has been presented [49].

Acknowledgments

This project was funded by BAP under Grant 09B501P. The author would like to thank Prof. Tereza Varnalı and Assoc. Prof. Şaron Çatak for helpful discussions. The author also thanks

Prof. Viktorya Aviyente and Assist. Prof. Başak Kayıtmazer for logistical support.

Disclosure statement

No potential conflict of interest was reported by the author.

Funding

This project was funded by BAP [grant number 09B501P].

ORCID

F. A. Akin http://orcid.org/0000-0001-9391-7026

References

[1] J. Cabalo and R. Sausa, Appl. Spectrosc. **57**, 1196 (2003).
[2] M. Greenfield, Y.Q. Guo, and E.R. Bernstein, Chem. Phys. Lett. **430**, 277 (2006).
[3] Y.Q. Guo, M. Greenfield, and E.R. Bernstein, J. Chem. Phys. **122**, 244310 (2005).
[4] Y.Q. Guo, M. Greenfield, A. Bhattacharya, and E.R. Bernstein, J. Chem. Phys. **127**, 154301 (2007).
[5] S. Bulusu, T. Axenrod, and G.W.A. Milne, Org. Mass Spectrom. **3**, 13 (1970).
[6] J. Stals, Trans. Faraday Soc. **67**, 1768 (1971).
[7] M. Farber, Mass Spectrom. Rev. **11**, 137 (1992).
[8] J. Yinon, Org. Mass Spectrom. **22**, 501 (1987).
[9] J. Yinon, D.J. Harvan, and J.R. Hass, Org. Mass Spectrom. **17**, 321 (1982); A. Gapeev, M. Sigman, and J. Yinon, Rapid Commun. Mass Spectrom. **17**, 943 (2003).
[10] S. Maharrey and R. Behrens, J. Phys. Chem. A **109**, 11236 (2005).
[11] A.P. Snyder, J.H. Kremer, S.A. Liebman, M.A. Schroeder, and R. A. Fifer, Org. Mass Spectrom. **24**, 15 (1989).
[12] R.G. Gillis, M.J. Lacey, and J.S. Shannon, Org. Mass Spectrom. **9**, 359 (1974).
[13] S.P. Sharma and S.C. Lahiri, Energetic Mater. **23**, 239 (2005).
[14] D. Chakraborty, R.P. Muller, S. Dasgupta, and W.A. Goddard III, J. Phys. Chem. A **104**, 2261 (2000).
[15] F.A. Akin and C.C. Jarrold, J. Chem. Phys. **118**, 1773 (2003).
[16] D.E. Spence, P.N. Kean, and W. Sibbett, Opt. Lett. **16**, 42 (1991).
[17] A. Zewail, editor, *The Chemical Bond: Structure and Dynamics* (Academic Press, New York, 1992).
[18] R.E. Russo, X. Mao, and S.S. Mao, Anal. Chem. **74**, 70 A (2002).
[19] O. Ingo´lfsson and A.M. Wodtke, J. Am. Soc. Mass Spectr. **12**, 1339 (2001).
[20] I.F. Shishkov, T.L. Elfimova, and L.V. Vilkov, J. Struct. Chem. **33**, 34 (1992).
[21] R.J. Karpowicz and T.B. Brill, J. Phys. Chem. **88**, 348 (1984).
[22] C. Chang and M.K. Gilson, J. Comp. Chem. **24**, 1987 (2003).
[23] C.S. Choi and E. Prince, Acta Crystallogr. Sect. B **28**, 2857 (1972).
[24] A.D. Becke, J. Chem. Phys. **98**, 5648 (1993).
[25] Y. Zhao and D.G. Truhlar, J. Phys. Chem. A **108**, 6908 (2004).
[26] Y. Zhao and D.G. Truhlar, J. Phys. Chem. A **109**, 5656 (2005).
[27] H.L. Schmider and A.D. Becke, J. Chem. Phys. **108**, 9624 (1998).
[28] M.J. Frisch, G.W. Trucks, H.B. Schlegel, G.E. Scuseria, M. A. Robb, J.R. Cheeseman, J.A. Montgomery, T. Vreven Jr., K.N. Kudin, J.C. Burant, J.M. Millam, S.S. Iyengar, J. Tomasi, V. Barone, B. Mennucci, M. Cossi, G. Scalmani, N. Rega, G. A. Petersson, H. Nakatsuji, M. Hada, M. Ehara, K. Toyota, R. Fukuda, J. Hasegawa, M. Ishida, T. Nakajima, Y. Honda, O. Kitao, H. Nakai, M. Klene, X. Li, J. E. Knox, H.P. Hratchian, J.B. Cross, V. Bakken, C. Adamo, J. Jaramillo, R. Gomperts, R.E. Stratmann, O. Yazyev, A.J. Austin, R. Cammi, C. Pomelli, J.W. Ochterski, P.Y. Ayala, K. Morokuma, G.A. Voth, P. Salvador, J.J. Dannenberg, V.G. Zakrzewski, S. Dapprich, A.D. Daniels, M.C. Strain, O. Farkas, D. K. Malick, A.D. Rabuck, K. Raghavachari, J.B. Foresman, J.V. Ortiz, Q. Cui, A.G. Baboul, S. Clifford, J. Cioslowski, B.B. Stefanov, G. Liu, A. Liashenko, P. Piskorz, I. Komaromi, R.L. Martin, D.J. Fox, T. Keith, M. A. Al-Laham, C.Y. Peng, A. Nanayakkara, M. Challacombe, P. M. W. Gill, B. Johnson, W. Chen, M.W. Wong, C. Gonzalez, and J.A. Pople, *Gaussian 003* (Gaussian, Inc0., Wallingford, CT, 2004).
[29] J.P. Merrick, D. Moran, and L. Radom, J. Phys. Chem. A **111**, 11683 (2007).
[30] S. Katsumata, H. Shiromaru, K. Mitani, S. Iwata, and K. Kimura, Chem. Phys. **69**, 423 (1982).
[31] D.P. Chong, D.C. Frost, W.M. Lau, and C.A. McDowell, Chem. Phys. Lett. **90**, 332 (1982).
[32] D.C. Frost, C.A. McDowell, and N.P.C. Westwood, J. Electron. Spectrosc. Relat. Phenom. **10**, 293 (1977).
[33] M.G. White, R.J. Colton, T.H. Lee, and J.W. Rabalais, Chem. Phys. **8**, 391 (1975).
[34] K.M. Ervin, J. Ho, and W.C. Lineberger, J. Phys. Chem. **92**, 5405 (1988).
[35] S.G. Lias, R.D. Levin, and S.A. Kafafi, in *NIST Chemistry WebBook*, edited by P.J. Linstrom W.G. Mallard (National Institute of Standards and Technology, Gaithersburg, MD, 2016), D. E. Clemmer and P. B. Armentrout, *J. Chem. Phys.* **97**, 2451 (1992); G. P. Bryant, Y. Jiang, M. Martin, and E. R. Grant, *ibid.* **101**, 7199 (1994).
[36] M. Xie, Z. Zhou, Z. Wang, D. Chen, F. Qi, Int. J. Mass Spectrom. **303**, 137 (2011).
[37] Y.Q. Guo, A. Bhattacharya, and E.R. Bernstein, J. Phys. Chem. A **113**, 85–96 (2009).
[38] W.H. Fink, J. Chem. Phys. **54**, 2911 (1971).
[39] E. Andersen and J. Simons, J. Chem. Phys. **66**, 2427 (1977).
[40] P.A. Benioff, J. Chem. Phys. **68**, 3405 (1978).
[41] Y. Morino, M. Tanimoto, S. Saito, E. Hirota, R. Awata, and T. Tanaka, J. Mol. Spectrosc. **98**, 331 (1983).
[42] K.H. Hellwege A.M. Hellwege, editors, *Book Landolt-Bornstein: Group II: Atomic and Molecular Physics: Structure Data of Free Polyatomic Molecules* (Springer-Verlag, Berlin, 1976), Vol. 7.
[43] E. Herbst, T.A Patterson, and W.C. Lineberger, J. Chem. Phys. **61**, 1300 (1974).

[44] A. Bhattacharya and E.R. Bernstein, J. Phys. Chem. A **115**, 4135 (2011).
[45] J.F. Arenas, J.C. Otero, D. Pelaez, and J. Soto, J. Chem. Phys. **119**, 7814 (2003).
[46] J. Florián, L. Gao, V. Zhukhovskyy, D.K. MacMillan, and M.P. Chiarelli, J. Am. Soc. Mass Spectrom. **18**, 835 (2007).
[47] Y. A. Jeilani, K. A. Duncan, D. S. Newallo, A. N. Thompson, and N. K. Bose, Rapid Commun. Mass Spectrom. **29**, 802 (2015).
[48] V. Vizcaino, S.E. Huber, P. Sulzer, M. Probst, S. Denifl and P. Scheier, Eur. Phys. J. D **66**, 27 (2012).
[49] F.A. Akin, Mass spectral decomposition mechanisms of RDX isomers upon electron attachment and electron ionisation: a DFT study of normal mode activation incorporating Duschinsky rotations, Mol. Phys. (2016). <http://dx.doi.org/10.1080/ 00268976.2016.1229059 >.